Technical Note: Correction of geometric x-ray image intensifier distortion based on digital image correlation

Technical note: Correction of geometric X-ray image intensifier distortion based on digital image correlation

Running title: DIC based XRII distortion correction

Sanctorum, Joaquim[1],
Van Wassenbergh, Sam[2],
Aerts, Peter[2],
Dirckx, Joris[1]

1. Laboratory of Biophysics and Biomedical Physics, Department of Physics, University of Antwerp, Groenenborgerlaan 171, 2020 Antwerpen, Belgium.

2. Laboratory of Functional Morphology, Department of Biology, University of Antwerp, Universiteitsplein 1, 2610 Antwerpen, Belgium.

Corresponding author:

Joaquim Sanctorum
Universiteit Antwerpen, Dept. Physics
Groenenborgerlaan 171
B-2020 Antwerpen
Belgium
tel: +32 3 265 35 53
fax: +32 3 265 33 18
email: joaquim.sanctorum@uantwerpen.be

This article has been accepted for publication and undergone full peer review but has not been through the copyediting, typesetting, pagination and proofreading process, which may lead to differences between this version and the Version of Record. Please cite this article as doi: 10.1002/MP.13944

Abstract

Purpose: X-ray image intensifiers (XRIIs) inevitably produce images suffering from geometric distortion. Presently, various local and global methods exist to correct for these distortions. However, the performance of global methods is limited for dominant local distortions, and local methods tend to suffer from patch discontinuity and are generally sensitive to noise. In this paper, a novel local method is presented based on digital image correlation (DIC), which does not suffer from patch discontinuity and noise.

Methods: As DIC is a very accurate and robust technique to analyze deformations, it is our candidate of choice to outperform existing correction methods. The performance of our technique was first validated through distortion simulations. Next, it was validated experimentally for four different orientations of the XRII.

Results: A theoretical study on images suffering from a simulated distortion (including noise and blurring) yielded corrections with an average accuracy of (0.20 ± 0.04) pixels. We obtained experimental data with our 14" XRII (292 mm field of view), suffering from a maximum distortion between 9.6 mm and 12.9 mm, and an average distortion between (4.4 ± 1.3) mm and (6.1 ± 2.5) mm over the image field for the different orientations. For an adequate choice of the facet size in the DIC analysis (greater than 40 pixels), the weighted mean residual error of our method varied between (0.037 ± 0.003) mm and (0.054 ± 0.003) mm, regardless of the XRII orientation. The maximum residual error varied between 0.081 mm and 0.185 mm.

Conclusions: From the simulations, we concluded that the proposed technique is affected by neither Gaussian noise nor blurring. Furthermore, it is shown that our method can reach an accuracy that is on par with or better than the current standard tools. The novel method is fast, requires minimal operator intervention and can be fully automated.

Keywords: X-ray image intensifier, distortion correction, digital image correlation, DIC

I. Introduction

In biomechanical research, stereoscopic X-ray imaging is a valuable tool for motion analysis[1,2]. Although flat-panel detector systems are gaining in popularity in medical research, their limited framerate (30 frames per second for a-Si TFT flat panel detector in general[3]) is insufficient for monitoring fast movements, which are often highly relevant in biomechanical research. To this day, the number of stereoscopic XRII-based imaging systems has been growing exponentially in state-of-the-art biomechanical research labs[4] (for example in Brown University, Providence[5]), showing the need for reliable XRII distortion correction methods.

The main distortions present in the images have a radial or sigmoidal nature. The former is a result of detecting the X-rays on a curved input phosphor and projecting the image on a flat surface. The latter is due to electromagnetic interactions of the produced photo-electrons and the surrounding magnetic field[6] (mainly the geomagnetic field). Local distortions may also arise due to the interaction of the electrons with localized magnetic fields[7]. The distortions introduce errors in the quantitative assessment of the recorded X-ray images and must therefore be corrected.

In general, the distorted images are corrected by applying an image transformation. Depending on the nature of the distortion pattern, this transformation must either be the same for the entire image or vary locally over the image field, resulting in a global or local correction method respectively. Considerable efforts have been made over the past two decades to develop global[7–12], local[13,14] and hybrid[15,16] techniques to correct for the image distortion.

The majority of the reported correction methods share a common fundament, namely the imaging of a rectilinear grid in the form of opaque markers, intersections of metal wires or a perforated plate. Due to the XRII distortion, the position of these markers will deviate from their expected position in the recorded image. Generally, a relation is established between the deviating and expected positions in the form of polynomial dewarping functions on a global or local level (or a combination of both, yielding a hybrid technique). It was shown in previous studies (Gronenschild[13], Fahrig *et al.*[9], Liu *et al.*[10]) that, in general, an increase in the order of the dewarping polynomials will result in an improvement of the accuracy of global correction methods. This is only true for an order up to six or seven since higher-order polynomials tend to fit the noise. Moreover, global methods only perform well if the distortions are highly non-local (which is often the case).

Local methods, on the other hand, are generally more sensitive to noise, exhibit patch-discontinuity between the local corrections areas[13] and often rely on the assumption of a distortion-free image center[11].

To overcome the issue of patch-discontinuity, Yan *et al.*[14] implemented a local technique based on moving least squares, at the expense of higher noise sensitivity.

Efforts have been made by Soimu *et al.*[15] and Yan *et al.*[16] to merge the benefits of global and local techniques in so-called hybrid methods. The method presented by Soimu *et. al.* allows the user to make a trade-off between computation time and correction accuracy, depending on the percentage of the image that is corrected locally. The fully local method yielded the most accurate results, at a greater computational cost. The results of Yan *et. al.* showed that their hybrid method based on multilevel B-spline approximation was 10% to 20% more accurate than the standard global and local methods they considered.

In this work, a novel local method for the distortion correction is presented, which does not suffer from patch discontinuity or noise corruption, and additionally does not rely on the assumption of a distortion-free image center. The method is based on an entirely different technique, namely Digital Image Correlation (DIC). DIC is a well-established optical non-contact technique for full-field analysis of 2D or 3D object deformations and is widely used in the field of structural mechanics. One of the main applications of DIC is the quantitative, full-field analysis of tensile tests on materials or biological tissues[17,18]. In the present paper, DIC will be applied to X-ray images using a custom DIC pattern mask. A description of the principles of DIC and the use of DIC within the proposed method is given in section II. In sections III and IV, the results of the method are shown and discussed. The description, results, and discussion of a theoretical study based on distortion simulations can be found in the supplementary material (Suppl_mat.pdf).

II. Materials and methods

A. Digital image correlation

Digital image correlation is an optical measurement technique, which is used to determine displacement and strain fields on the surface of deformed objects. To this end, an image of the object is recorded in its original state, followed by an image (series) of the deformed object. The possibility to correlate the deformed images to the original image is enabled by applying a random speckle pattern to the object's surface. It is then assumed that the deformation of the speckle pattern as seen in the images is the same as the deformation of the surface reflecting that pattern[19].

To carry out a DIC analysis, a rectilinear grid is defined on the image, of which the spacing is governed by the grid step parameter. Next, a facet (or subset) of gray values, which has a square shape in our case, is considered around each of the grid points. We will refer to the length of the sides of the square facets as the facet size. As the object is deformed, the applied random speckle pattern will be deformed accordingly and as a result, the subsets of gray values are displaced and distorted in the images. Based on the random gray value distribution within the subsets, each of the original subsets is identified in the deformed images,

immediately yielding the coordinates of the corresponding subset in the deformed image. Therefore, using DIC analysis, the relation between the original and distorted coordinates is retrieved directly. Various methods exist to perform the correlation analysis[20], however, the common fundament is a correlation criterion to evaluate the degree of similarity between the original and deformed subsets. In our study, the correlation is performed in ISTRA 4D software version 4.4.6 (Dantec Dynamics GmbH, Ulm, Germany).

To translate this optical technique to X-ray imaging, a custom binary pattern of randomly placed circles was designed in Matlab (Mathworks, Massachusetts, USA). The circles have radii varying between 1 mm and 3 mm. As shown in Fig. 1, the pattern is built out of nine identical segments, containing randomly sampled circles, and L-shaped reference holes in each of the segment centers. These reference holes are used to determine the orientation of the pattern and the scaling of the pattern on the digitized image. The pattern was laser cut (Raytech, Belgium) in the center of a $500 \times 500 \times 0{,}5$ mm plate of stainless steel (AISI 304) with a tolerance of 0,10 mm. By imaging this pattern using an XRII, the pattern will be distorted, and this distortion is analyzed using DIC. Because the laser cutting process might introduce errors in the pattern, a high contrast optical image of the laser cut pattern was taken and binarized. This way, the reference image in the DIC analysis will be closest to the ground truth pattern.

B. Distortion correction

In general, image distortion can be formulated as a positional change of the undistorted image coordinates, denoted as x_u and y_u:

$$\begin{aligned} x_d(x_u,y_u) &= x_u + \delta_x(x_u,y_u) \\ y_d(x_u,y_u) &= y_u + \delta_y(x_u,y_u) \end{aligned} \tag{1}$$

where δ_x and δ_y denote the position-dependent distortion surfaces, which define the relation between undistorted and distorted coordinates (referred to using subscript d). In case the distortion surfaces are known, the gray values of the corrected image can be retrieved by evaluating the distorted image in the distorted coordinates:

$$I_c(x_u,y_u) = I_d(x_d(x_u,y_u),y_d(x_u,y_u)) \tag{2}$$

where I_c and I_d represent the corrected and distorted image respectively. The main goal of the distortion correction method is thus to find the unknown distortion surfaces to establish the relation between the undistorted and distorted coordinates. As DIC analysis is being widely used to measure full-field deformations, it is our candidate of choice to directly retrieve the distorted coordinate surfaces $x_d(x_u,y_u)$ and $y_d(x_u,y_u)$.

The distortion correction is carried out in a few steps, which are schematically shown in Fig. 2. As the DIC analysis is based on the comparison of gray values in the original (binary) and deformed image (12bit), the

raw X-ray image is not adequate as input for the algorithm. Therefore, the X-ray image is first segmented and binarized (after flat field and log correction). Then, the binarized image and the original digital pattern are used as input to perform the DIC analysis, directly yielding the distorted coordinate surfaces of the facets under consideration, denoted as $x_d(x'_u,y'_u)$ and $y_d(x_u',y'_u)$. In former expressions, x'_u and y_u' depict the indices of the grid points on which the DIC analysis was performed, which depend on the chosen grid step. In theory, the grid step can be taken as one pixel to perform the analysis for each pixel separately. As the image consists of 2048 × 2048 pixels, the DIC analysis would then take a tremendous amount of time. Since the distortion is a smooth function of distance, it suffices to determine the displacement maps on a much coarser grid, for example, every 16 pixels.

It may occur that for some of the sample points, the DIC analysis is not successful and no distorted coordinate value is calculated, introducing missing data in the distorted coordinate surfaces. This typically occurs when a small facet size is chosen as in that case the gray value subset may not contain enough data to be uniquely identified in the deformed image. Therefore, the missing data is estimated by carrying out 2D linear scattered data interpolation on this dataset and linear extrapolation is carried out at the endpoints. Afterward, the distorted coordinate surfaces are rescaled to the full image size using 2D linear gridded data interpolation, yielding the distorted surfaces $x_d(x_u,y_u)$ and $y_d(x_u,y_u)$. The gray values of the corrected images are finally retrieved using equation (2). However, $x_d(x_u,y_u)$ and $y_d(x_u,y_u)$ are generally non-integer values which do not correspond to integer pixel locations. Therefore, to retrieve the gray values of the corrected image, it is necessary to interpolate between the gray values of the distorted image at the locations given by the elements of x_d and y_d. In this work, the gray values of the corrected image are estimated using 2D linear interpolation.

C. Image acquisition and experimental procedure

The X-ray images were acquired using a Philips Imagica HC 36cm (14") image intensifier (Philips, Eindhoven, The Netherlands) connected to a Photron FastCam Mini WX50-32GB (Photron, Tokyo, Japan) with a frame rate of 750fps. The CMOS detector of the camera contains 2048 × 2048 pixels with a pixel size of 10x10µm. A Philips SRM 0511 ROT 500 x X-ray tube was used to generate the X-rays. The field of view was taken as large as possible, to maximize the effect of distortion, yielding a field of view of 292 × 292 mm (pixel size $\approx$ 0.143 mm).

X-ray images of the laser cut pattern were recorded under four different orientations of the image intensifier, namely $\alpha = \{0°,30°, 60°,90°\}$ with respect to the horizontal plane and the distorted coordinate surfaces were retrieved as formerly described. Also, for each orientation under consideration, 11 X-ray images of a rectilinear grid were taken. In our study, the dependence of the quality of the correction on the XRII orientation and the size of the correlation subsets was examined. The rectilinear grid consisted of 11

× 11 steel markers with a diameter of 2 mm and a center-to-center spacing of 25 mm. The holes of the rectilinear grid were cut with a CNC machine with a tolerance of 0.05 mm.

The 44 images of the distorted rectilinear pattern were corrected using our DIC technique and the centers of the markers (denoted as x_k^{corr} and y_k^{corr}) were extracted using standard center-of-mass coordinate (centroid) computation. To these center coordinates, the best fitting rectilinear grid was calculated using the quasi-Newton BFGS-method, yielding the ideal grid positions x_k^{fit} and y_k^{fit}. A suitable measure for the accuracy of the correction method would be the Euclidian distance between the corrected and the fitted center locations (denoted as R_k):

$$R_k = \sqrt{\left(x_k^{corr} - x_k^{fit}\right)^2 + \left(y_k^{corr} - y_k^{fit}\right)^2} \quad (3)$$

The maximum, mean and standard deviation of the set $\{R_k\}$ will be used to present the accuracy of the correction method. Since the simulations showed the dependence of the quality of the correction on the facet size used in the DIC analysis (Fig. S-4), the DIC analysis was carried out for a facet size of {25, 29, 33, … 93} pixels. The grid step was kept constant at 16 pixels since the simulations showed no improvement of the method for more densely sampled distortion surfaces (Fig. S-3).

III. Results

For each of the XRII orientations, the rectilinear grid was imaged 11 times, after imaging the DIC pattern. Using DIC analysis, the distorted coordinate surfaces were retrieved and used to correct the images of the rectilinear grid. In Fig. 3, an example of the result of the corrected grid is shown, along with the spatial distribution of the residual errors.

After the correction, the residual errors (R_k) were calculated using Eq. (3). In Fig. 4, the spread of the mean and maximum residual errors (R_{mean} and R_{max}) within the series of the 11 images for each XRII orientation are shown in function of the facet size used in the correlation. For each XRII orientation, our results are summarized in Table 1. In this table, we only considered the data obtained for an adequate choice of the used facet size, which is greater than 40 pixels (see Fig. 4). The mean values reported in the table ($\langle R_{mean} \rangle$) were calculated by taking the weighted mean of the mean residual errors of the 11 images over the range of facet sizes greater than 40 pixels, yielding 154 data points per XRII orientation. Regardless of the XRII orientation, the weighted mean residual error varies between (0.26 $\pm$ 0.02) pixels and (0.38 $\pm$ 0.02) pixels, corresponding to (0.037 $\pm$ 0.003) mm and (0.054 $\pm$ 0.003) mm. Considering the full angle range, our method is accurate up to (0.294 $\pm$ 0.007) pixels on average, corresponding to (0.042 $\pm$ 0.001) mm.

IV. Discussion

By comparing panels **(a)** and **(b)** of Fig. 3, one can see that the distortion present in the image is successfully corrected (the white lines are perfectly straight). As shown in panel **(c)**, the distribution of the residual errors is mostly random. It is shown in Table 1 that an overall average accuracy of (0.294 ± 0.007) pixels can be reached, corresponding to approximately (0.042 ± 0.001) mm. Furthermore, the difference in average accuracy for the 11 images corresponding to the same orientation is less than 5-10%, proving the robustness and reproducibility of the method. As can be seen from the lower four panels of Fig. 4, the maximum error is generally close to or less than 1 pixel.

As mentioned, we used a fixed grid step of 16 pixels for the DIC analysis. In a preliminary study, we discovered that a grid step in the range of 4 to 80 pixels did not notably affect the average accuracy of the method. For example, for an image in the $\alpha = 30°$ set, using a fixed facet size of 61 pixels in the DIC analysis, the mean residual error varied between 0.236 pixels and 0.254 pixels over the considered range of grid steps. Increasing the grid step sped up the process, but introduced an increased amount of missing data on the image periphery and a slight increase in the maximum error could be noticed. On the other hand, decreasing the grid step considerably increased the correlation time, without an increase in accuracy. A grid step of 16 pixels provides an excellent balance between correlation time, information at the image periphery and maximum error.

To compare the quality of our method to the existing tools, an accuracy given in pixels is not sufficient since the size of a pixel depends on the imaging field of view and the number of pixels in the image. Therefore, it is more correct to compare the accuracy using units of distance. As the amount of distortion strongly depends on the diameter of the XRII and the imaging field of view, the accuracy of a correction method will depend on these as well. It was for example shown by Fantozzi *et al.*[11] (2003) that, generally, the error of a correction method increases with the size of the XRII. In order to compare our method to the existing tools, we need to take this dependency into account.

Methods have been tested on a 9" XRII by Gronenschild[8] (1997), Liu *et al.*[10] (1999), Yan *et al.*[14] (2007) and Yan *et al*[16]. (2011). In the first two works, global methods were presented with an accuracy in the range of 0.03 mm to 0.05 mm, which is also in agreement with the results of Fantozzi *et al.* for a field of view of 220 mm. The hybrid method reported in the work of Yan *et.al.* (2011) was more accurate than their formerly reported local one (2007) and a standard global method, reaching an accuracy of approximately 0.25 pixels. However, considering the fact their images were digitized with 21 pixels/cm, this corresponds to an accuracy of approximately 0.12 mm, which is beyond the range reached by Gronenschild and Liu *et. al.*.

Soimu *et al.*[15] (2003) and Meng *et al.*[12](2014) presented their results using a 12" XRII. In the former work, a hybrid method was presented, reaching an accuracy of 0.077 mm. However, depending on the percentage

of the image that is locally corrected, the accuracy may differ[15]. The latter work presented a global method reaching an accuracy of 0.34 pixels. However, since the image consists of 512 × 512 pixels, the performance is rather limited. Fahrig *et al.*[9] (1997) presented a global method that reached an accuracy of 0.04 mm using a field of view of 270 mm.

Larger XRIIs were considered in the works of Fantozzi *et al.* and Gutiérrez *et al.*[7] (2008). The team of Fantozzi presented a global method based on thin-plate splines, reaching an accuracy of 0.057 mm for a 320 mm field of view. Gutiérrez *et al.* presented an efficient method to estimate the distortion for an arbitrary orientation of the C-arm (similar to Liu *et al.*). For an arbitrary value of the primary angle α, an accuracy of 0.22 pixels could be reached, corresponding to approximately 0.14 mm for a 330 mm field of view. The large variety of correction methods and their accuracy as summarized above will serve as a reference for the accuracy of the method presented in this work.

Our weighted mean residual error varied between (0.037 ± 0.003) mm and (0.054 ± 0.003) mm, regardless of the XRII orientation. This closely corresponds to the range reached by Gronenschild and Liu *et. al.*, yet the size of our XRII is considerably larger. The overall weighted mean residual error of (0.042 ± 0.001) mm matches the result obtained by Fahrig *et. al.*. Considering the large size of our XRII (14") and the field of view (292 mm), our new method matches the existing methods and outperforms a number of them.

The first results of our method are promising, yet some limitations remain. One of them is the laser cutting of the pattern, as this might introduce differences in the pattern with respect to the originally designed digital one. We have partly overcome this issue by also taking a high-contrast optical image of the pattern to be used for the DIC analysis. However, lens distortions cannot be fully excluded. Secondly, DIC software is needed to use our method. These DIC software packages are often expensive, which can be a drawback. However, open-source alternatives exist, making the technique very accessible. We were unable to verify our experimental results using these alternatives due to their functionality being limited to DIC patterns which, unlike ours, are completely random. Finally, it was reported by Sutton *et. al.*[17] and Pan *et.al.*[19] that decorrelation in the DIC analysis occurs for a relative rotation between the original and deformed facet of 10° or more, making identification of the deformed facet impossible. However, since the maximum rotational distortion in the X-ray images is of the order of a few degrees, the decorrelation itself is limited, still enabling the identification of the deformed facets. This decorrelation will only be a problem if the DIC mask is placed against the surface of the XRII under a large angle. Therefore, we recommend attaching the DIC mask as level as possible to assure the limited decorrelation.

V. Conclusions

A novel method to correct for the geometric distortion of image intensifiers based on digital image correlation was developed and verified. A theoretical study based on various simulations promised highly sub-pixel accurate results for both small and large distortions. The simulations also demonstrated that the proposed technique is affected by neither Gaussian image noise nor blurring. Additionally, our presented local method does not suffer from patch discontinuity and does not rely on the assumption of a distortion-free image center. Our experimental results show that, regardless of the XRII orientation, the weighted mean residual error lies between (0.037 $\pm$ 0.003) mm and (0.054 $\pm$ 0.003) mm, and an average overall accuracy of (0.042 $\pm$ 0.001) mm was reached for our 14" XRII. The maximum residual error varied between 0.57 pixels and 1.30 pixels, corresponding to 0.081 mm and 0.185 mm. By comparing our method to existing literature, we showed that our method matches existing methods and outperforms a number of standard tools.

Acknowledgments

Wim Huyge is acknowledged for constructing the rectilinear pattern and the mounting system of the laser cut DIC pattern. We would also like to acknowledge Marek Lomnitz of Dantec Dynamics for the support in using the ISTRA 4D software. This research was funded by a grant from the special research fund of the University of Antwerp (BOF-GOA 2016 33927).

Conflict of Interest Statement

The authors have no conflicts to disclose.

References

1. Camp AL, Roberts TJ, Brainerd EL. Swimming muscles power suction feeding in largemouth bass. *Proceedings of the National Academy of Sciences*. 2015;112(28):8690-8695. doi:10.1073/pnas.1508055112

2. Brainerd EL, Baier DB, Gatesy SM, et al. X-ray reconstruction of moving morphology (XROMM): precision, accuracy and applications in comparative biomechanics research. *Journal of Experimental Zoology Part A: Ecological Genetics and Physiology*. 2010;313A(5):262-279. doi:10.1002/jez.589

3. Weisfield R, Colbeth R, Mollov I, Ganguly A. X-ray imager with CMOS sensor embedded in TFT flat panel. March 2017. https://patents.google.com/patent/US9588235B2/en. Accessed December 4, 2018.

4. Orenstein. Brown's influential biomechanics X-ray technology grows ever more powerful. https://phys.org/news/2016-12-brown-influential-biomechanics-x-ray-technology.html. Accessed October 2, 2019.

5. X-ray Reconstruction of Moving Morphology (XROMM). https://www.xromm.org/. Accessed July 26, 2019.

6. Bushong SC. *Radiologic Science for Technologists: Physics, Biology, and Protection*. 11th ed. St. Louis, Missouri: Elsevier; 2017.

7. Gutiérrez LF, Ozturk C, McVeigh ER, Lederman RJ. A practical global distortion correction method for an image intensifier based x-ray fluoroscopy system. *Medical Physics*. 2008;35(3):997-1007. doi:10.1118/1.2839099

8. Gronenschild E. The accuracy and reproducibility of a global method to correct for geometric image distortion in the x-ray imaging chain. *Medical Physics*. 1997;24(12):1875-1888. doi:10.1118/1.598101

9. Fahrig R, Moreau M, Holdsworth DW. Three-dimensional computed tomographic reconstruction using a C-arm mounted XRII: Correction of image intensifier distortion. *Medical Physics*. 1997;24(7):1097-1106. doi:10.1118/1.598013

10. Liu RR, Rudin S, Bednarek DR. Super-global distortion correction for a rotational C-arm x-ray image intensifier. *Medical Physics*. 1999;26(9):1802-1810. doi:10.1118/1.598684

11. Fantozzi S, Cappello A, Leardini A. A global method based on thin-plate splines for correction of geometric distortion: An application to fluoroscopic images. *Medical Physics*. 2003;30(2):124-131. doi:10.1118/1.1538228

12. Meng C, Zhang J, Zhou F, Wang T. New method for geometric calibration and distortion correction of conventional C-arm. *Computers in Biology and Medicine*. 2014;52:49-56. doi:10.1016/j.compbiomed.2014.06.009

13. Gronenschild E. Correction for geometric image distortion in the x-ray imaging chain: Local technique versus global technique. *Medical Physics*. 1999;26(12):2602-2616. doi:10.1118/1.598800

14. Yan S, Wang C, Ye M. A method based on moving least squares for XRII image distortion correction. *Medical Physics*. 2007;34(11):4194-4206. doi:10.1118/1.2791037

15. Soimu D, Badea C, Pallikarakis N. A novel approach for distortion correction for X-ray image intensifiers. *Computerized Medical Imaging and Graphics*. 2003;27(1):79-85. doi:10.1016/S0895-6111(02)00055-1

16. Yan S, Nie S, Zheng B. Improving accuracy of XRII image distortion correction using a new hybrid image processing method: Performance assessment. *Medical Physics*. 2011;38(11):5921-5932. doi:10.1118/1.3644846

17. Sutton MA, Orteu J-J, Schreier H. *Image Correlation for Shape, Motion and Deformation Measurements*. Boston, MA: Springer US; 2009. doi:10.1007/978-0-387-78747-3

18. Palanca M, Tozzi G, Cristofolini L. The use of digital image correlation in the biomechanical area: a review. *International Biomechanics*. 2016;3(1):1-21. doi:10.1080/23335432.2015.1117395

19. Pan B, Qian K, Xie H, Asundi A. Two-dimensional digital image correlation for in-plane displacement and strain measurement: a review. *Measurement Science and Technology*. 2009;20(6):062001. doi:10.1088/0957-0233/20/6/062001

List of figure captions

Fig. 1: **(a)** Binarized optical image of the laser cut speckle pattern. **(b)** A single segment out of which the pattern is built, containing the L-shaped reference hole in the center. **(c)** The laser cut pattern. **(d)** X-ray image of the laser cut pattern.

Fig. 2: Schematic representation of the distortion correction method. First, the X-ray image of the pattern is segmented. Second, the DIC analysis is performed, yielding the subsampled distorted coordinate surfaces $x_d(x'_u,y'_u)$ and $y_d(x_u',y_u')$. Third, the distorted coordinate surfaces are interpolated (and extrapolated) on a coarse scale using 2D linear scattered data interpolation. Then, the surfaces are resampled to the full image

size using 2D linear gridded data interpolation, yielding $x_d(x_u,y_u)$ and $y_d(x_u,y_u)$. Finally, the distorted coordinate surfaces are used to correct the distorted images

Fig. 3: **(a)** Original image of the rectilinear grid at $\alpha = 30°$ orientation. **(b)** Corresponding corrected image. **(c)** Corresponding residual error (R_k) distribution. The gray cross-shaped markers show the position of the corrected grid point and the black arrows show the magnitude and orientation of the residual error. The residual errors varied between 0.0003 pixels and 0.59 pixels, corresponding to 0.00004 mm and 0.084 mm respectively.

Fig. 4: The top and bottom rows respectively show the spread of the mean and maximum errors within the series of 11 images for each XRII orientation (indicated in the top right corner of each panel). The black line denotes the mean value of the error within the series, the gray region marks out the maximum and minimum (mean) error. The results are shown in function of the used facet size.

Table 1: Experimental results

$\alpha(°)$	$\langle R_{mean} \rangle$ (pixels)	R_{max} (pixels)	R_{min} (pixels)
0	0.38 ± 0.02	[0.87 , 1.30]	[0.0008 , 0.0896]
30	0.26 ± 0.02	[0.57 , 1.06]	[0.0003 , 0.0560]
60	0.30 ± 0.02	[0.62 , 0.94]	[0.0021 , 0.0608]
90	0.29 ± 0.02	[0.63 , 1.20]	[0.0013 , 0.0606]
Overall	0.294 ± 0.007	[0.57 , 1.30]	[0.0003 , 0.0896]

Summary of our experimental results for each of the XRII orientations (given by the angle α) for an adequate choice of the facet size (greater than 40 pixels). For each orientation the weighted mean of the mean residual errors ($\langle R_{mean} \rangle$) over the 11 images and the range of facet sizes is presented, along with the range of the maximum and minimum residual errors (R_{max} and R_{min}). The bottom row contains the overall weighted mean residual error over the full angle range, along with the corresponding range of maximum and minimum residual error.

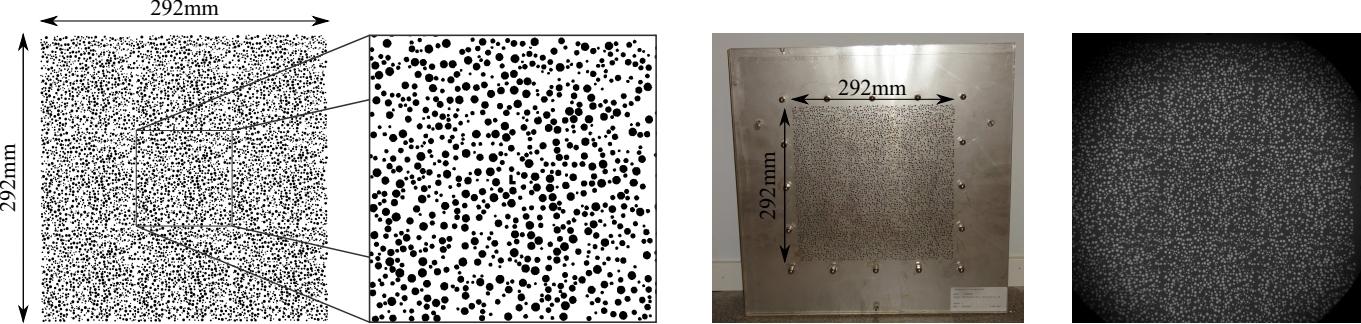

(a) (b) (c) (d)

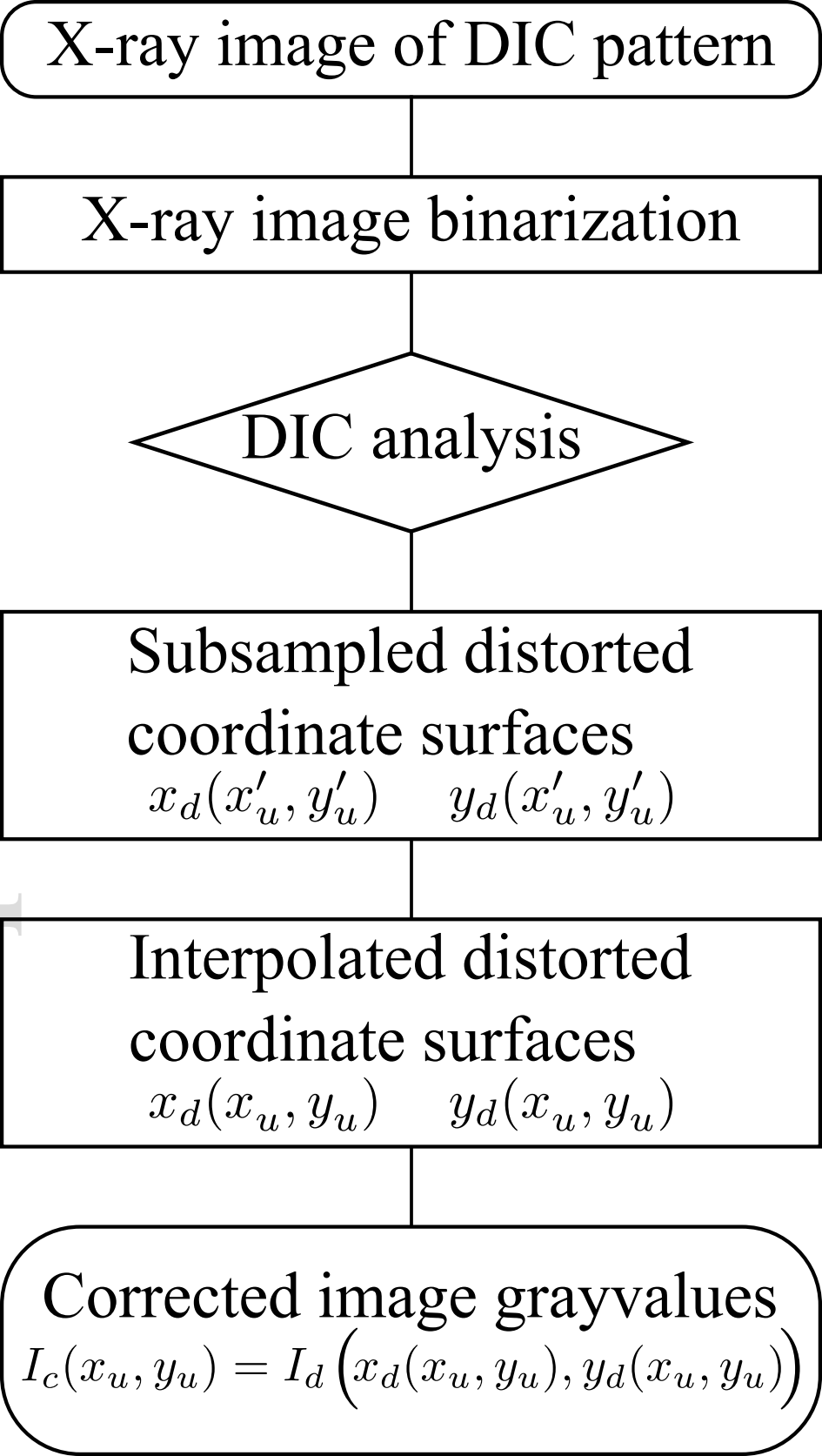
X-ray image of DIC pattern
X-ray image binarization
DIC analysis
Subsampled distorted coordinate surfaces
$x_d(x'_u, y'_u)$ $y_d(x'_u, y'_u)$
Interpolated distorted coordinate surfaces
$x_d(x_u, y_u)$ $y_d(x_u, y_u)$
Corrected image grayvalues
$I_c(x_u, y_u) = I_d\left(x_d(x_u, y_u), y_d(x_u, y_u)\right)$

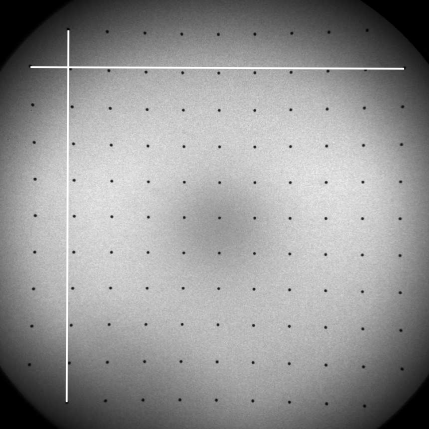

(a)

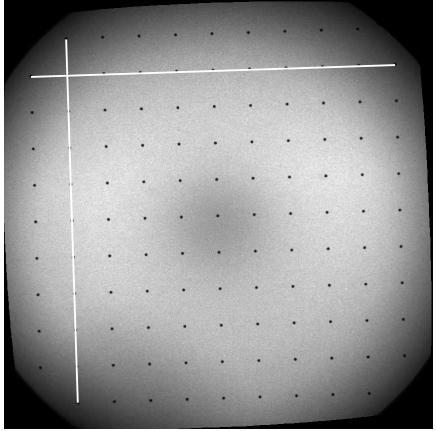

(b)

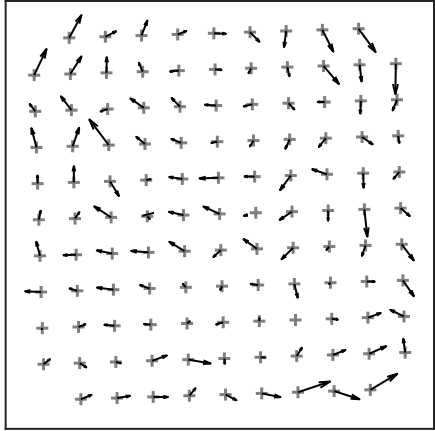

(c)

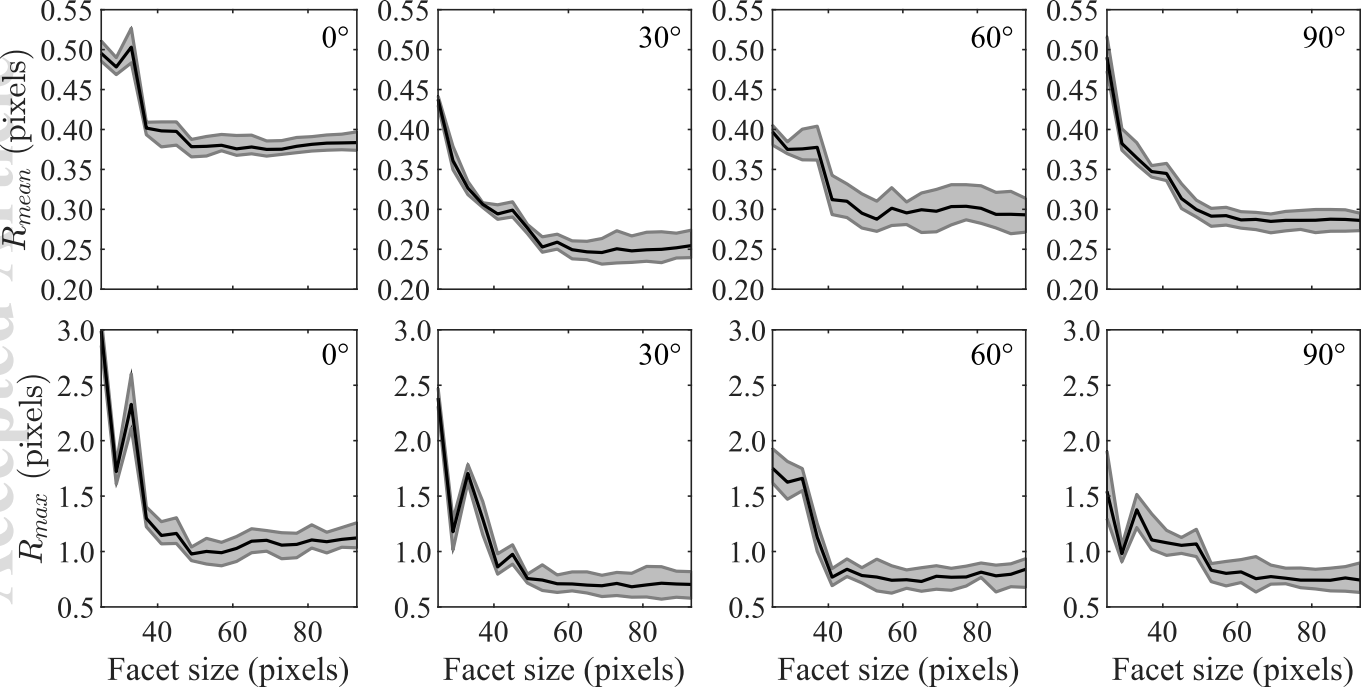
0°
30°
60°
90°
R_{mean} (pixels)
R_{max} (pixels)
Facet size (pixels)
Facet size (pixels)
Facet size (pixels)
Facet size (pixels)